



ARTICLE

Desired Dynamic Equation for Primary Frequency Modulation Control of Gas Turbines

Aimin Gao¹, Xiaobo Cui^{2,*}, Guoqiang Yu¹, Jianjun Shu¹ and Tianhai Zhang¹

¹Thermal Power Center, Jiangsu Frontier Electric Technology Co., Ltd., Nanjing, 211102, China

²School of Energy and Power Engineering, Nanjing Institute of Technology, Nanjing, 211167, China

*Corresponding Author: Xiaobo Cui. Email: xiaobo@njit.edu.cn

Received: 08 September 2023 Accepted: 23 November 2023 Published: 30 April 2024

ABSTRACT

Gas turbines play core roles in clean energy supply and the construction of comprehensive energy systems. The control performance of primary frequency modulation of gas turbines has a great impact on the frequency control of the power grid. However, there are some control difficulties in the primary frequency modulation control of gas turbines, such as the coupling effect of the fuel control loop and speed control loop, slow tracking speed, and so on. To relieve the abovementioned difficulties, a control strategy based on the desired dynamic equation proportional integral (DDE-PI) is proposed in this paper. Based on the parameter stability region, a parameter tuning procedure is summarized. Simulation is carried out to address the ease of use and simplicity of the proposed tuning method. Finally, DDE-PI is applied to the primary frequency modulation system of an MS6001B heavy-duty gas turbine. The simulation results indicate that the gas turbine with the proposed strategy can obtain the best control performance with a strong ability to deal with system uncertainties. The proposed method shows good engineering application potential.

KEYWORDS

Gas turbine; primary frequency modulation (PFM); desired dynamic equation (DDE); proportion-integral (PI)

1 Introduction

Due to the advantages of fast response, high efficiency, and cleanliness, gas turbine units are becoming a key component in building new-type power system in China. In order to cope with the load and frequency fluctuations caused by the large-scale integration of new energy power sources such as photovoltaic power and wind power into the power grid, gas turbine units need to have a strong primary frequency modulation (PFM) capability, which are of great significance for the safe operation and frequency stability of the power grid.

In order to further enhance the PFM capability of gas turbine units, many scholars have conducted extensive research in terms of control strategy designs, control logic optimizations, and other aspects. In reference [1], a medium-pressure heating throttling scheme was proposed to optimize the PFM logic in order to increase the margin of load regulation for gas turbine units. In reference [2], a significant improvement in the response speed of the unit's PFM was achieved by optimizing the speed control mode of the main control system, reducing the frequency modulation dead-zone and increasing the frequency modulation amplitude. In reference [3], the response speed of the unit to PFM commands



was improved by adding locking logic and modifying frequency difference signals. For the problem that the response index of the PFM cannot meet the requirements of the power grid, an optimization logic scheme based on feedforward limiting and compensation for power closed-loop was proposed in reference [4] to improve the PFM capability.

The actual control logic of PFM in gas turbines is mostly based on the Proportional-Integral (PI) control strategy [5], due to the advantages of PI controllers, such as simple structure, excellent performance, simple implementation, and clear parameter meanings [6]. In addition, in order to further enhance the PFM capability of gas turbines, a new method based on Active Disturbance Rejection Control (ADRC) was proposed in reference [7], where ADRC parameters are optimized through a multi-objective genetic algorithm to achieve the improvement of gas turbine PFM capability. In addition, control strategies based on neural networks are also studied in the PFM system of gas turbines [8]. Due to the large amount of computation requirements for advanced control strategies, their engineering implementation still faces certain challenges. However, there is still no lack of potential for large-scale engineering applications given the arithmetic capabilities of current gas turbine control platforms [9]. For a long time in the future, the PI control strategy will still occupy the dominant position in the PFM system of gas turbines [10]. To enhance the control performance of PI in the PFM system of gas turbines, it is necessary to optimize the structure and parameter tuning of PI controllers. The DDE-PI controller has received increasing attention due to its adjustable parameters with feedforward coefficients, which can effectively balance the contradiction between tracking and anti-disturbance performance of closed-loop systems [11]. The DDE-PI controller further enhances the robustness of the closed-loop system while retaining the advantages of the classical PI strategy, and has been well applied in the super-heated steam temperature system [12] and the high-pressure heater water level system [13]. Running data show that DDE-PI has strong application potential.

In this study, a DDE-PI control strategy for the PFM system of a gas turbine is designed. Firstly, the composition of the MARK V heavy-duty gas turbine PFM system is introduced, and the control characteristics of the system are analyzed. Then, the DDE-PI control strategy is introduced, the calculation of the parameter stability domain is provided, and the practical parameter tuning procedure is summarized. Next, the DDE-PI control strategy proposed in this study is applied to the PFM control of MARK V heavy-duty gas turbine units. The simulation results show that the gas turbine unit using the method proposed in this study can ensure optimal PFM capability and a strong ability to cope with system uncertainty. Finally, the work of this study is summarized.

2 PFM Model of MS6001B Heavy-Duty Gas Turbine

A frequency modulation system of an MS6001B heavy-duty gas turbine based on the MARK V control system was introduced in reference [14]. Taking the speed control system, fuel control system, and acceleration control system into consideration, the structural diagram of the PFM control system is shown in Fig. 1, where the acceleration control speed is generally kept constant in the control system. Reference [14] provides the physical meanings and corresponding values of some model parameters in Fig. 1, as shown in Table 1. The models of the other links are as follows:

$$G_T(s) = \frac{3.3s + 1}{450s} \quad (1)$$

$$G_{z1}(s) = \frac{1}{2.5s + 1} \quad (2)$$

$$G_{z2}(s) = \frac{2}{15s + 1} + 0.5 \tag{3}$$

In addition, the controllers for speed and fuel in the system are $G_1(s)$ and $G_2(s)$, respectively. $G_1(s)$ and $G_2(s)$ can choose many control strategies, such as PI and ADRC.

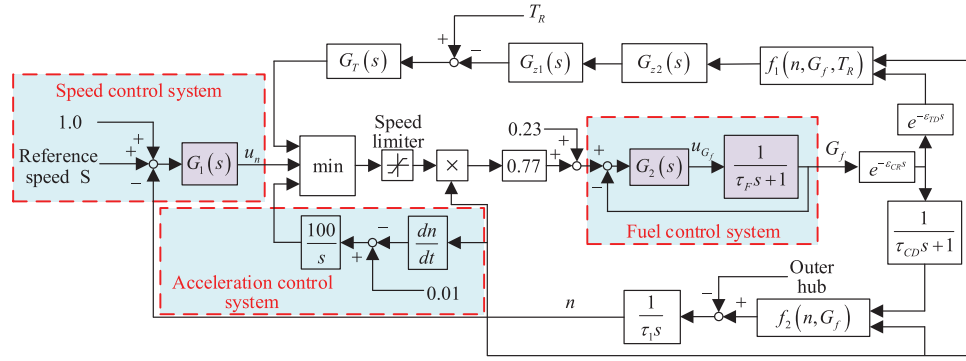


Figure 1: PFM control model of an MS6001B heavy-duty gas turbine

Table 1: The physical meaning and numerical values of related model parameters

Symbol	τ_1	τ_F	τ_{CD}	ϵ_{CR}	ϵ_{TD}
Physical meaning	Turbine rotor time constant	Fuel system time constant	Compressor displacement time constant	Combustion reaction delay	Exhaust system transportation delay
Value	18.5	0.1	0.10	0.01	0.02

The system model is built based on a liquid-fueled circulating single-shaft gas turbine, with a rated speed of 5100 r/min and rated power of 359 MW. The exhaust temperature, rated inlet temperature, and speed governing droop of the gas turbine unit are 550°C, 15°C, and 4%, respectively [5].

From Fig. 1, the output of the fuel control system of the gas turbine goes through a pure lag link and an inertia link. Combined with the integration effect, the speed of the gas turbine is obtained and serves as the output value of the speed control system, which is algebraically calculated as the set value of the fuel control system. This means that there is a coupling effect between the speed control system and the fuel control system due to their interaction. Note that G_f and n are fuel quantity and speed, respectively, and role as controlled variables. u_{G_f} and u_n are valve opening and unit speed of the PFM system, respectively, and role as manipulated variables. In addition, $T_R = 550^\circ\text{C}$ means the exhaust temperature. To enhance the control performance of the gas turbine PFM system, this study optimizes the parameters in Fig. 1, starting from the design of the control strategy.

3 Desired Dynamic Equation PI (DDE-PI) Controller

Consider a general system described by the following equation:

$$G_p(s) = \Delta \frac{\alpha_0 + \alpha_1 s + \dots + \alpha_{p-q-1} s^{p-q-1} + s^{p-q}}{\beta_0 + \beta_1 s + \dots + \beta_{p-1} s^{p-1} + s^p} e^{-\tau s} \tag{4}$$

where p , q and τ are the denominator order, the relative order and the high-frequency gain of the system, respectively. $\alpha_j (j = 1, 2, \dots, p - q - 1)$ and $\beta_k (k = 1, 2, \dots, p - 1)$ are the coefficients of the numerator and denominator of the system transfer function, respectively. Considering system uncertainty, α_j , β_k and Δ are generally uncertain or unknown.

The following state space form is obtained by the state transformation of Eq. (4):

$$\begin{aligned} \dot{\phi}_j &= \phi_{j+1} \\ \dot{\phi}_j &= -\sum_{j=0}^{q-1} \lambda_j \phi_{j+1} - \sum_{j=0}^{p-q-1} \varsigma_j \varphi_{j+1} + \Delta u, j = 1, \dots, q-1 \\ \dot{\phi}_j &= \varphi_{j+1} \\ \dot{\phi}_{p-q} &= -\sum_{j=0}^{p-q-1} \alpha_j \varphi_{j+1} + \phi_1, j = 1, \dots, p-q-1 \\ y &= \phi_1 \end{aligned} \quad (5)$$

where $\phi_j (j = 1, 2, \dots, q)$ and $\varphi_j (j = 1, 2, \dots, p - q)$ are the state variables of the system. $\lambda_i (i = 1, 2, \dots, q - 1)$ and $\varsigma_i (i = 1, 2, \dots, p - q - 1)$ are unknown parameters.

Define the observation extended state as:

$$f(\phi, \varphi, u) = -\sum_{j=0}^{q-1} \lambda_j \phi_{j+1} - \sum_{j=0}^{p-q-1} \varsigma_j \varphi_{j+1} + (\Delta - l) u \quad (6)$$

where l is a parameter whose positive or negative sign is consistent with the symbol Δ . $\dot{\phi}_q$ in Eq. (5) can be described by the following equation:

$$\dot{\phi}_q = f(\phi, \varphi, u) + lu \quad (7)$$

when the relative order of the controlled object q equals 2, Eq. (5) is transformed to:

$$\begin{cases} \dot{\phi}_1 = \phi_2 \\ \dot{\phi}_2 = f(\phi, \varphi, u) + lu \\ y = \phi_1 \end{cases} \quad (8)$$

The DDE strategy for the closed-loop system is designed as:

$$\ddot{y} + h_1 \dot{y} + h_0 y = r \quad (9)$$

Combining Eq. (8), it can be obtained that the designed control law is:

$$u = \frac{-h_0(\phi_1 - r) - h_1 \phi_2 - \hat{f}}{l} \quad (10)$$

where \hat{f} is the observer's observation of the extended state $f(\phi, \varphi, u)$, and can be estimated using the disturbance observer down below [15]:

$$\begin{cases} \dot{\hat{f}} = \theta + k\phi_2 \\ \dot{\theta} = -k\theta - k^2\phi_2 - klu \end{cases} \quad (11)$$

where k and θ are the gain and intermediate variables of the disturbance observer, and Eq. (10) is equivalent to:

$$\begin{aligned}
 u &= \frac{-h_0(\phi_1 - r) - h_1\phi_2 - \hat{f}}{l} \\
 &= -\frac{\theta + k\phi_2 + h_0(\phi_1 - r) + h_1\phi_2}{l}.
 \end{aligned} \tag{12}$$

Considering the disturbance observer in Eq. (11), it can be obtained that:

$$\dot{\theta} = -k\theta - k^2\phi_2 - klu = k[h_0(\phi_1 - r) + h_1\phi_2] \tag{13}$$

Eq. (14) can be obtained by integrating both sides of Eq. (13).

$$\theta = -k \left[h_0 \int (\phi_1 - r) dt + h_1\phi_1 \right] \tag{14}$$

Considering Eqs. (13), (14) is equivalent to:

$$u = -\frac{k \left[h_0 \int (\phi_1 - r) dt + h_1\phi_1 \right] + k\phi_2}{l} - \frac{h_0(\phi_1 - r) + h_1\phi_2}{l} \tag{15}$$

Considering that the set value r undergoes a step change in the actual system, \dot{r} is infinite and generally set to zero. Then we can get the tracking error as $e = r - \phi_1$ and $\dot{e} = \dot{r} - \dot{\phi}_1 = -\dot{\phi}_2$, Eq. (15) is equivalent to:

$$u = \underbrace{\frac{kh_1 + h_0}{l}}_P e + \underbrace{\frac{kh_0}{l}}_I \int e dt + \underbrace{\frac{k + h_1}{l}}_D \dot{e} - \frac{kh_1}{l} r \tag{16}$$

Similarly, when the controlled object turns out to be a system with a relative order of 1, its control law can be obtained as:

$$u = \underbrace{\frac{k + h_0}{l}}_P e + \underbrace{\frac{kh_0}{l}}_I \int e dt - \frac{k}{l} r \tag{17}$$

Thus, it is known that PI/PID control based on DDE is a two-degree freedom structure containing a feedforward and feedback controller, which is shown in Fig. 2 [16], b_f is the feedforward controller and $b_f = \frac{k}{l}$ (PI) or $b_f = \frac{kh_1}{l}$ (PID). $G_c(s)$ is the feedback controller and $G_c(s) = k_p + \frac{k_i}{s}$ (PI) or $G_c(s) = k_p + \frac{k_i}{s} + k_d s$ (PID).

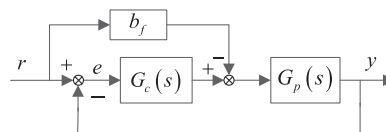


Figure 2: Control structure of DDE-PI/PID

Since differentiation introduces amplification of the manipulated variable by measurement noise, DDE-PI controllers are adopted as $G_1(s)$ and $G_2(s)$ for the PFM system of MARK V heavy-duty gas turbine in this study.

4 Parameter Tuning of DDE-PI Controller

According to the Mason transformation formula, the closed-loop system transfer function from r to y can be obtained as:

$$G(s) = \frac{y(s)}{r(s)} = \frac{(G_c(s) - b) G_p(s)}{1 + G_c(s) G_p(s)} \quad (18)$$

As is shown in Eq. (17), the feedforward controller does not appear in the characteristic equation of the closed-loop system, that is to say b_f does not affect the stability of the system, the stability only depends on the feedback controller $G_c(s)$ and the controlled object $G_p(s)$.

The frequency domain response of the controlled object described in Eq. (4) is depicted as follows [17]:

$$G_p(j\omega) = r(\omega) e^{i\theta(\omega)} = a(\omega) + jb(\omega) \quad (19)$$

where ω , $a(\omega)$ and $b(\omega)$ represent the angular frequency, real and imaginary parts of the controlled object, respectively.

The stability domain of the DDE-PI controller can be obtained using the D-partitioning method. The stability domain boundary of PI controller includes nonsingular boundary ∂D_ω when $\omega \in (0, -\infty) \cup (0, +\infty)$, and singular boundary ∂D_0 and ∂D_∞ when $\omega = 0$, $\omega = \pm\infty$ [18], respectively. By solving the stability domain boundary equations separately, the stability region of PI controller parameters can be obtained:

$$\begin{cases} K_i = 0 \\ \omega + K_p a(\omega) \omega + K_i b(\omega) = 0 \\ K_p b(\omega) \omega + K_i a(\omega) = 0 \end{cases} \quad (20)$$

Combining $k_p = \frac{k + h_0}{l}$ and $k_i = \frac{kh_0}{l}$, and taking $l \neq 0$ into consideration, the stability region of the DDE-PI controller can be obtained:

$$\begin{cases} kh_0 = 0 \\ l\omega + (k + h_0) a(\omega) \omega + kh_0 b(\omega) = 0 \\ (k + h_0) b(\omega) \omega + kh_0 a(\omega) = 0 \end{cases} \quad (21)$$

The parameters of the DDE-PI controller should be reasonably selected from the stability region described in Eq. (21). Through extensive simulations, the parameter tuning procedure is summarized as follows:

1. Determine the coefficients of the desired dynamic PI equation $\dot{y} + h_0 y = r$ according to control performance requirements. For example, given the desired adjustment time t_{sd} , $h_0 \in [4 \sim 12] / t_{sd}$ is obtained;
2. Choose a larger l and $k \in [3 \sim 10] h_d$;
3. Reduce l value until satisfactory control performance is achieved;
4. If satisfactory control performance cannot be achieved, repeat step 2 to step 3 with appropriate increase of h_0 .

The parameter tuning procedure of the DDE-PI controller is shown in Fig. 3. It can be observed that the proposed tuning procedure has strict logic and simple steps even though it needs trials and errors.

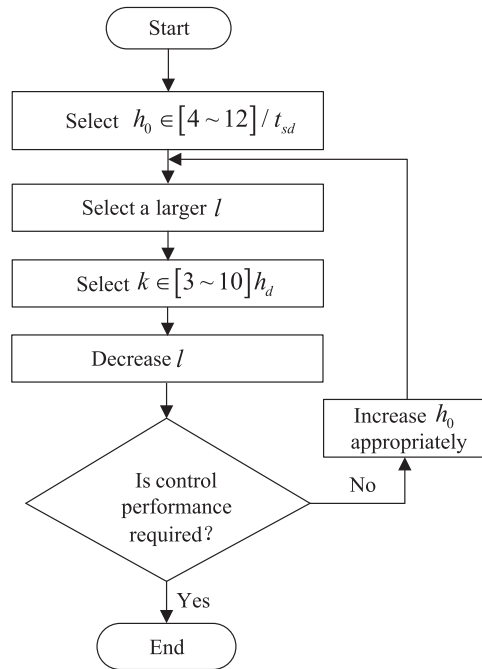


Figure 3: Parameter tuning procedure of DDE-PI

To illustrate the simplicity and effectiveness of the proposed tuning method, take $G_p(s) = \frac{1}{2.5s + 1}e^{-0.3s}$ in Eq. (2) as an example. Fig. 4 presents the stability region of the DDE-PI controller.

The stability region provides the range of parameter selection, and then the tuning procedure above can be applied to obtain satisfactory parameters. The selected parameters of the DDE-PI controller are $t_{sd} = 3$, $k = 0.5$, $l = 5$ and $h_0 = 15$. As a comparative controller, PI is tuned as $K_p = 2$ and $K_I = 1$. Fig. 5 shows the control performance for $G_p(s) = \frac{1}{2.5s + 1}e^{-0.3s}$, it can be learned that DDE-PI

controller can obtain faster tracking performance and better disturbance rejection ability. To compare the control performance under different conditions, Monte Carlo experimental method is applied to test controller robustness [19]. By perturbing parameters of $G_p(s)$ within $\pm 20\%$ range of their nominal values, one can obtain control performance with uncertain systems as shown in Figs. 6 and 7, it can be observed that the DDE-PI still obtains better control performance for uncertain systems. This discussion explains how to obtain the parameters of DDE-PI and illustrates the advantages of DDE-PI, and this provides a good foundation for the following applications for the gas turbine PFM system.

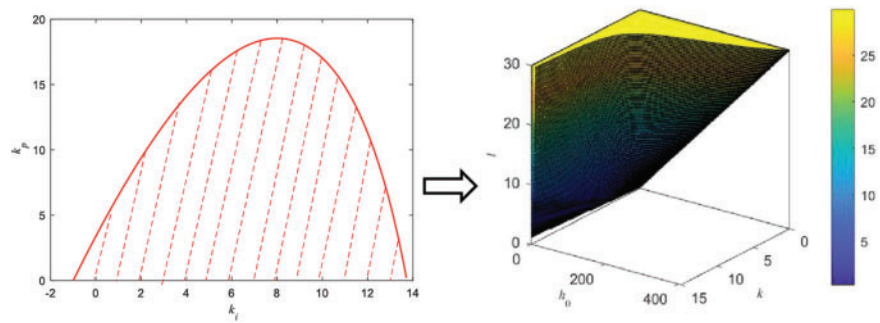


Figure 4: The stability region of DDE-PI for $G_p(s) = \frac{1}{2.5s + 1}e^{-0.3s}$ (Left: the stability region $\{k_p, k_i\}$ of DDE-PI, Right: the stability region $\{k, l, h_0\}$ of DDE-PI)

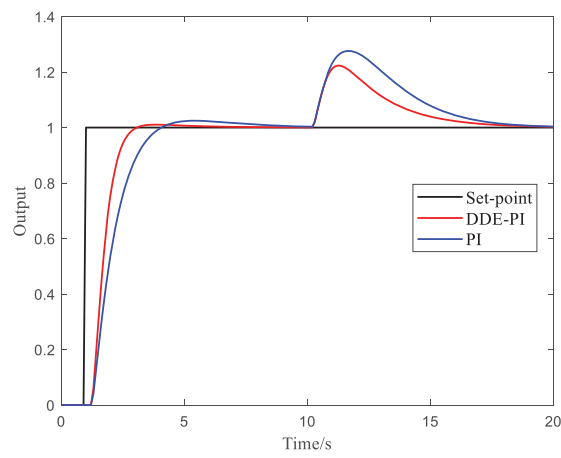


Figure 5: The control performance of DDE-PI for $G_p(s) = \frac{1}{2.5s + 1}e^{-0.3s}$

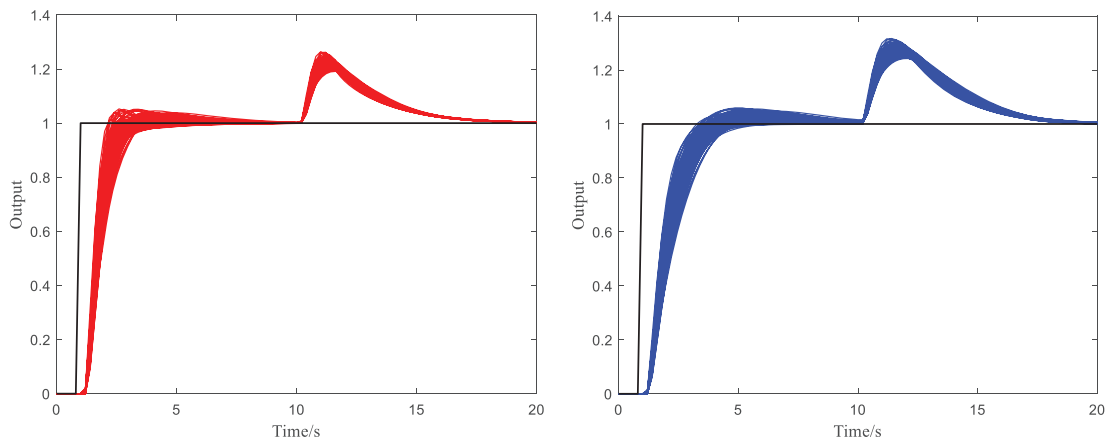


Figure 6: The control performance of DDE-PI and PI for uncertain systems (Left: DDE-PI, Right: PI)

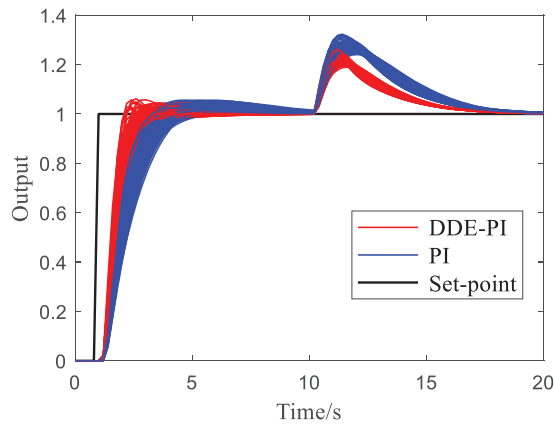


Figure 7: The control performance of DDE-PI and PI for uncertain systems in one figure

5 Simulation verification

The DDE-PI controller proposed in this section will be applied to the gas turbine PFM system shown in Fig. 1, both $G_1(s)$ and $G_2(s)$ are DDE-PI controllers. The multi-objective optimized ADRC and PI control strategies designed in reference [7] are chosen as comparison control strategies. The three control strategies are denoted as DDE-PI, multi-objective optimized ADRC, and multi-objective optimized PI, respectively. The parameters of all three control strategies are listed in Table 2.

Table 2: Controller parameter list

Controller	$G_1(s)$	$G_2(s)$
DDE-PI	$h_0 = 5,$ $k = 0.02,$ $l = 0.2$	$h_0 = 0.005,$ $k = 0.005,$ $l = 0.025$
Multi-objective optimized ADRC	$k_p = 5.102,$ $b_0 = 1.002,$ $\omega_o = 6.001,$ $\theta = 0.802$	$k_p = 5.102,$ $b_0 = 1.002,$ $\omega_o = 6.001,$ $\theta = 0.802$
Multi-objective optimized PI	$K_p = 4.052,$ $K_I = 0.099$	$K_p = 1.000,$ $K_I = 0.0011$

5.1 Control Performance Comparison under Nominal Working Conditions

Under nominal working conditions, i.e., the model parameters are the nominal parameters given in Section 2, the simulation results are obtained and shown in Figs. 8 and 9, the simulation settings are as follows: Under initial stable working conditions of the system, the PFM signal of the unit steps up at 100 s, that is at 100 s it rises by 0.0025 and then stabilizes; At 600 s, it rises again by 0.0025 and then stabilizes; At 1100 s, the speed drops by 0.0050 and then stabilizes. Note that the model established in Fig. 1 is in the form of a unit system, the value is 1 under nominal working conditions, and the values of parameters change on this basis.

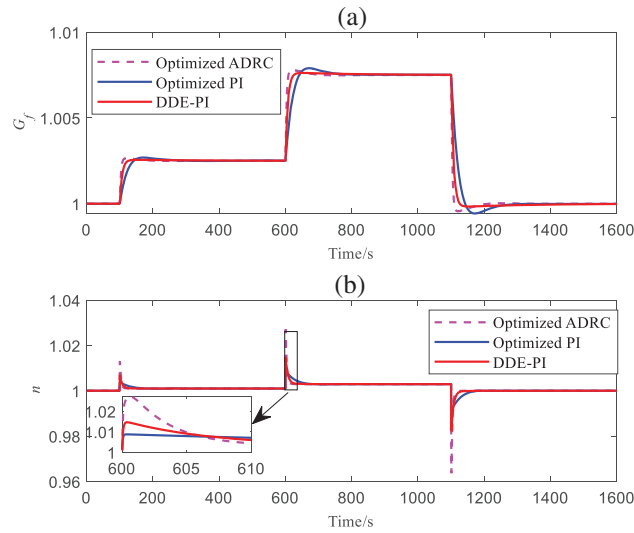


Figure 8: Outputs of G_f and n of the PFM system under nominal working conditions

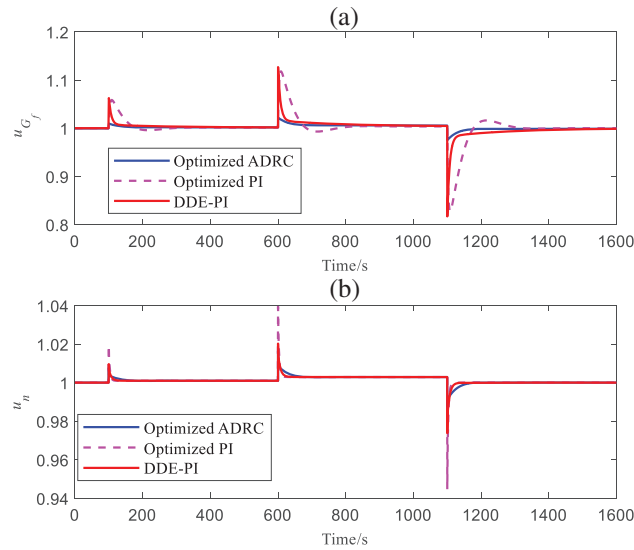


Figure 9: u_{G_f} and u_n of the PFM system under nominal working conditions

From Fig. 8a, the DDE-PI proposed in this study has the minimum overshoot, faster response than multi-objective optimized PI, and its response speed is very close to that of multi-objective optimized ADRC. From Fig. 8b, the overshoot of DDE-PI is smaller than that of multi-objective optimized ADRC, and only slightly larger than that of multi-objective optimized PI. However, the response speed of DDE-PI is much faster than that of multi-objective optimized PI. To better measure the control performance of three control strategies, define the following indexes:

$$J_1 = \int_{t=0}^{end} |G_f - G_{f0}| \tag{23}$$

$$J_2 = \int_{t=0}^{end} |n - n_{sp}| \quad (24)$$

where G_{f0} and n_{sp} are the set values for fuel quantity and PFM speed under steady-state operating conditions, respectively. Table 3 shows the maximum overshoots of G_f loop, J_1 and J_2 during each dynamic process. The above analysis has been further validated in Table 3. Considering J_1 , J_2 and minimum overshoot comprehensively, the DDE-PI control strategy has the best control performance.

Table 3: Control performance under nominal operating conditions

Control performance	J_1	Maximum overshoot of G_f loop (%)	J_2
DDE-PI	0.0824	0.41	0.2867
Multi-objective optimized ADRC	0.1184	5.86	0.3731
Multi-objective optimized PI	0.2073	2.27	0.2937

5.2 Control Performance Comparison under Uncertain Operating Conditions

Due to the change of dynamic parameters of the gas turbine model with working conditions, modeling simplification and other reasons, the system would have some uncertainties [20]. To measure the control performance of the above control strategies in the presence of system uncertainty, some dynamic parameters from $f_2(n, G_f)$ are selected and deviated by 20% from the design value, that is 80% of the original value. The results shown in Figs. 10 and 11 can be obtained while keeping the controller parameters unchanged. Although there is some uncertainty in the PFM system of gas turbines, DDE-PI strategy still has minimum overshoot, and its response speed is faster than that of multi-objective optimized PI while slightly slower than that of multi-objective optimized ADRC. It can be concluded that DDE-PI has a strong ability to deal with system uncertainties.

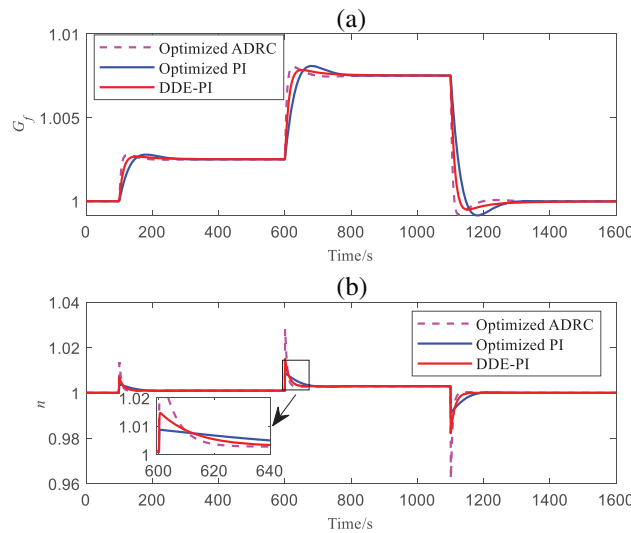


Figure 10: Outputs of G_f and n of the PFM system under uncertain working conditions

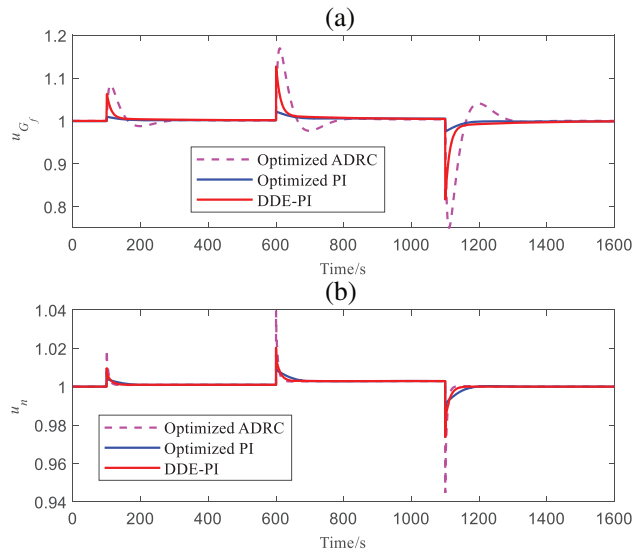


Figure 11: u_{G_f} and u_n of the PFM system under uncertain working conditions

To further compare the ability of control strategies to cope with the uncertainty of PFM systems, firstly, the dynamic parameters of the gas turbine, $f_1(n, G_f, T_R)$ and $f_2(n, G_f)$ listed in Table 1 are randomly perturbed within the range of $\pm 20\%$ of the original value, keeping parameters of the control strategies unchanged and the simulation was repeated 100 times as shown in Fig. 4, and the G_f and n output results of uncertain systems are shown in Figs. 12–14.

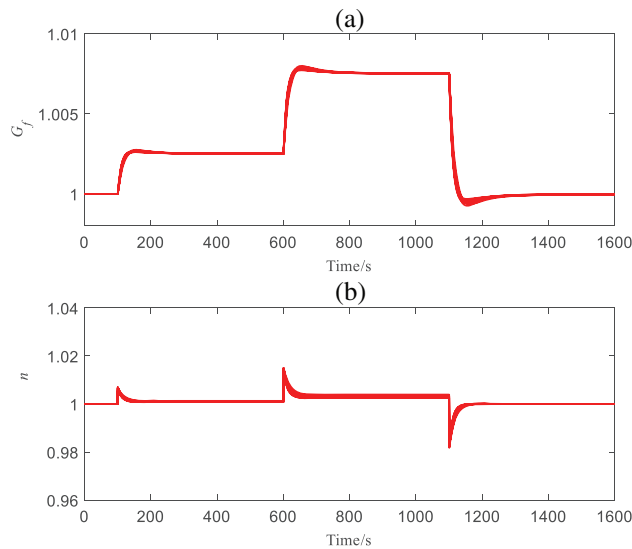


Figure 12: Outputs of G_f and n of the PFM system under uncertain working conditions with DDE-PI

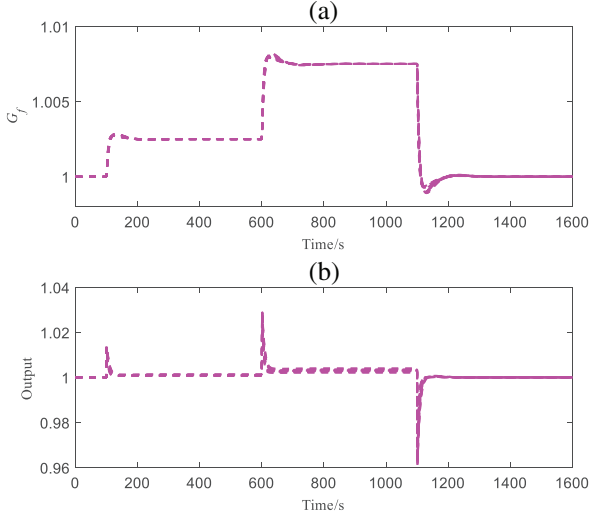


Figure 13: Outputs of G_f and n of the PFM system under uncertain working conditions with multi-objective optimized ADRC

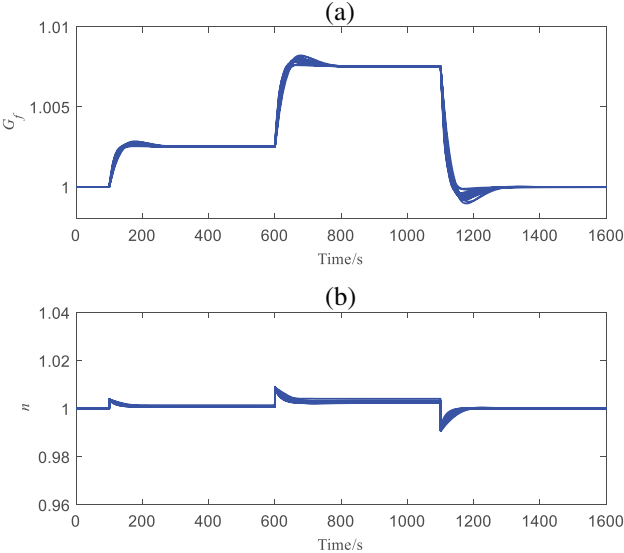


Figure 14: Outputs of G_f and n of the PFM system under uncertain working conditions with multi-objective optimized PI

From Figs. 12–14, DDE-PI can ensure that the MS6001B heavy-duty gas turbine PFM system maintains a relatively ideal control performance even in the presence of uncertainty, the output results of G_f and n are still able to be around the output of the nominal operating conditions, which means that DDE-PI has a strong capability to deal with system uncertainty. Similarly, multi-objective optimized ADRC also has a strong ability to cope with system uncertainty, while the output results of G_f and n are still able to be around the output of the nominal operating conditions, as is shown in Fig. 13. From Fig. 14, multi-objective optimized PI has the worst ability to cope with system uncertainty.

Through the above analysis, it can be concluded that DDE-PI has the best PFM capability while ensuring robustness, and has great potential for practical industrial applications.

6 Conclusions

In order to improve the PFM capability of gas turbines, a DDE-PI controller is proposed in this study to enhance the control performance of the PFM system. Firstly, a typical PFM model of an MS6001B heavy-duty gas turbine is introduced, and its control characteristics are analyzed. Next, the DDE-PI control strategy is introduced, and an easy-to-implement and highly engineered parameter tuning procedure is summarized. Finally, the DDE-PI control method is applied to the PFM system of an MS6001B heavy-duty gas turbine, the simulation results show that the DDE-PI control strategy can achieve smaller overshoot with a fast response, demonstrating strong engineering application value. Based on the theoretical and simulation analysis, the subsequent work will further validate the effectiveness of the proposed method by completing the on-site realization of control logic, logical protection, parameter tuning, and putting into operation on-site of DDE-PI for actual units.

Acknowledgement: We would like to thank all those who have contributed to this paper for their valuable assistance, and thanks for the support provided by Jiangsu Frontier Electric Technology Co., Ltd.

Funding Statement: This work is supported by Science and Technology Project of Jiangsu Frontier Electric Technology Co., Ltd. (Grant Number KJ202004), Gao A. M. (author who received the grant).

Author Contributions: The authors confirm their contribution to the paper as follows: study conception and design: Aimin Gao, Xiaobo Cui; data collection: Guoqiang Yu; simulation verification: Xiaobo Cui; analysis and interpretation of results: Aimin Gao, Jianjun Shu, Tianhai Zhang; draft manuscript preparation: Aimin Gao, Xiaobo Cui. All authors reviewed the results and approved the final version of the manuscript.

Availability of Data and Materials: The data that support the findings of this study are available from the corresponding author, upon reasonable request.

Conflicts of Interest: The authors declare that they have no conflicts of interest to report regarding the present study.

References

1. Ji, G. J., Jiang, Y. (2020). Optimization of primary frequency control strategy for gas turbines. *Thermal Turbine*, 49(4), 262–266.
2. Wu, H. B. (2012). Primary frequency regulation based optimization for control system of M701F gas-steam combined cycle power unit. *Thermal Power Generation*, 41(12), 61–64+67.
3. Xi, X. G., Sun, W. (2021). The optimization of primary frequency modulation on 9E gas turbine. *Gas Turbine Technology*, 34(3), 50–52+72.
4. Xiao, X. Y., Shi, Y. Y., Tang, K. Y., Gao, A. M., Zhang, T. H. (2022). Analysis and optimization on primary frequency control of an Ansaldo AE94.3A gas turbine. *Power Equipment*, 36(1), 71–74.
5. Wang, C., Liu, S. M. (2006). Simulation and discussion on primary frequency regulation of gas turbine. *Thermal Turbine*, 1, 23–26.

6. Chen, J. Q., Ma, D., Xu, Y., Chen, J. (2022). Delay robustness of PID control of second-order systems: Pseudo-concavity, exact delay margin, and performance trade-off. *IEEE Transactions on Automatic Control*, *67*(3), 1194–1209.
7. Shu, J. J., Cui, X. B., Yu, G. Q., Gao, A. M., Shi, Y. Y. et al. (2022). Active disturbance rejection control based on multi objective genetic algorithm for primary frequency modulation. *Science Technology and Engineering*, *22*(3), 1068–1075.
8. Deng, Q. C., Liu, S. M., Sun, H. (2015). Effect of gas turbine feed forward neural networks on primary frequency regulation. *Thermal Turbine*, *44*(2), 127–132.
9. Du, S. L., Zhang, Q. D., Cao, B. Q., Qiao, J. F. (2022). A review of model predictive control for urban wastewater treatment process. *Information and Control*, *51*(1), 41–53.
10. Cheng, T., Zeng, Z. Z., Du, X. F., Wang, F. Q., Cheng, Q. Z. (2019). Predictive self-coupling PI control method for large time-delay systems. *Information and Control*, *48*(6), 672–677.
11. Wang, W. J., Li, D. H., Gao, Q. R., Wang, C. F. (2008). A two degree-of-freedom PID controller tuning method. *Journal of Tsinghua University (Science and Technology)*, *11*, 1786–1790.
12. Xue, Y., Li, D., Liu, J. (2010). DDE-based PI controller and its application to gasifier systems temperature control. *International Conference on Control, Automation and Systems*, pp. 2194–2197. Gyeonggi-do, Korea.
13. Shi, G. J., Liu, S. J., Li, D. H., Ding, Y. J., Chen, Y. Q. (2022). A controller synthesis method to achieve independent reference tracking performance and disturbance rejection performance. *ACS Omega*, *7*(18), 16164–16186.
14. Liu, S. M., Wang, C. (2004). Analysis and discussion on primary frequency regulation of gas turbine and combined cycle. *Thermal Turbine*, *33*(3), 154–157.
15. Tornambe, A. (1994). A decentralized controller for the robust stabilization of a class of MIMO dynamical systems. *Journal of Dynamic Systems, Measurement, and Control*, *116*, 293–304.
16. Somefun, O. A., Akingbade, K., Dahunsi, F. (2021). The dilemma of PID tuning. *Annual Reviews in Control*, *52*, 65–74.
17. N'Doye, I., Asiri, S., Aloufi, A., Al-Awan, A., Laleg-Kirati, T. (2020). Intelligent proportional-integral-derivative control-based modulating functions for laser beam pointing and stabilization. *IEEE Transactions on Control Systems Technology*, *28*(3), 1001–1008.
18. Shafiei, Z., Shenton, A. T. (1994). Tuning of PID-type controllers for stable and unstable systems with time delay. *Automatica*, *30*(10), 1609–1615.
19. Xiang, S. W., Fan, H. Q., Fu, Q. (2021). Error distribution of zero-effort miss distance under mode mismatch. *International Journal of Control*, *94*(3), 643–652.
20. Wu, Z. L., Li, D. H., Chen, Y. Q. (2020). Active disturbance rejection control design based on probabilistic robustness for uncertain systems. *Industrial & Engineering Chemistry Research*, *59*(40), 18070–18087.